PERGAMON

International Journal of Solids and Structures 37 (2000) 7145–7159

INTERNATIONAL JOURNAL OF SOLIDS and STRUCTURES

www.elsevier.com/locate/ijsolstr

Stochastic aspects of localised failure: material and boundary imperfections

M.A. Gutiérrez, R. De Borst *

Faculty of Aerospace Engineering, Koiter Institute Delft, Delft University of Technology, P.O. Box 5058, NL-2600 GB Delft, Netherlands

Received 30 July 1999; in revised form 1 February 2000

Abstract

This paper presents the application of the finite element reliability method to the evaluation of the statistical properties of localisation phenomena. Material and boundary constraint imperfections are considered. The latter are imposed through Lagrange multipliers. The evaluation of the sensitivity to the stochastic basic variables, which is needed in the reliability method, is outlined. Numerical simulations of mode-I and mode-II localisation phenomena are presented. © 2000 Elsevier Science Ltd. All rights reserved.

Keywords: Stochastic aspects; Localised failure; Boundary imperfection

1. Introduction

When failure of solids and structures is simulated, difficulties appear that cast doubt on the validity of the results. On one hand, classical continuum models become physically meaningless when material deterioration leads to a progressive stress reduction (softening behaviour). This can be remedied by means of enhanced continuum models (De Borst et al., 1993), which stem from a better understanding of the degradation phenomena. On the other hand, failure of solids can take place suddenly in states of homogeneous deformation. As the actual failure mechanism is often initiated by heterogeneity in the material, computer simulations cannot reproduce this behaviour unless an imperfection is manually supplied somewhere in the solid.

Incorporation of heterogeneity in the mathematical model requires the use of random quantities. A meaningful technique for this purpose is the finite element reliability method of Der Kiureghian and Ke (1988), in which the response statistics are analysed by means of probability approximations at the likely configurations of imperfections. For the particular case of localisation analysis, this method has been applied successfully to study the effect of stochastic distributions of strength and other material properties (Gutiérrez, 1999; Gutiérrez and De Borst, 1999a,b).

Another possible source of imperfections in a structure can be the loading system. For the particular case of experimental set-ups, excentricity or horizontality errors in the loading platens can lead to erroneous

* Corresponding author. Tel.: +31-15-278-5464; fax: +31-15-261-1465.
E-mail address: r.deborst@lr.tudelft.nl (R. De Borst).

PII: S0020-7683(00)00193-1

conclusions on the mechanical behaviour of the analysed specimen. In order to simulate the influence of these errors numerically, stochastic quantities can be introduced in the description of the loading system.

The loading system is usually modelled as a set of affine boundary constraints. Affine boundary constraints have traditionally been imposed through transformation matrices in the finite element equations. This method can be troublesome when the involved degrees of freedom are affected by more than one constraint (Schreyer and Parsons, 1995). Other possibilities (Barlow, 1982) are the penalty method, which can be inaccurate, and the Lagrange-multiplier method, which is regarded as costly from a computational point of view. The advent of efficient solution techniques for sparse systems of equations has led to a revaluation of the Lagrange-multiplier method as a versatile technique to impose affine constraints, with application to linear as well as non-linear problems (Rodríguez-Ferran and Huerta, 1999). The formal simplicity of the Lagrange-multiplier method makes it possible to introduce a stochastic description of the boundary constraints in a straightforward manner, and thus to carry out reliability computations, which account for imperfections of the loading system.

This paper is outlined as follows: after a brief introduction of the finite element reliability method, the evaluation of the equilibrium path in presence of affine constraints imposed through Lagrange multipliers is formulated. Then, the computation of the sensitivity of the equilibrium path to the material properties and boundary constraints, which is needed in the reliability method, is treated for the particular case of path-dependent material models. Application examples of mode-I as well as of mode-II localisation phenomena are presented.

2. The finite element reliability method

The equilibrium path of a solid Ω in quasi-static loading conditions is furnished by any pair of processes $(\mathbf{u}, \mathbf{t})$, representing the displacement field and the boundary traction field, respectively, that satisfies the equations

$$\begin{aligned} \nabla\boldsymbol{\sigma} &= 0 \text{ in } \Omega, \\ \boldsymbol{\sigma} &= \mathscr{F}(\boldsymbol{\varepsilon}, \mathbf{w}) \text{ in } \Omega, \\ \boldsymbol{\varepsilon} &= \frac{1}{2}\left[\mathbf{u}\nabla + (\mathbf{u}\nabla)^{\mathrm{T}}\right] \text{ in } \Omega, \\ \mathbf{u} &= \hat{\mathbf{u}} \text{ in } \Omega_c \subset \Omega \cup \partial\Omega, \\ \boldsymbol{\sigma}^{\mathrm{T}}\mathbf{n} &= \mathbf{t} \text{ in } \partial\Omega_t \subset \partial\Omega \end{aligned} \tag{1}$$

at any instant τ. In this equation, the processes $\boldsymbol{\varpi}$ and $\boldsymbol{\varepsilon}$ represent the stress and strain fields, $\mathbf{w}$ are the material properties, $\mathscr{F}$ represents a function in general, $\hat{\mathbf{u}}$ are prescribed affine constraints, $\mathbf{n}$ is the outward normal vector of $\partial\Omega$ and T represents the transpose symbol. Body forces have been neglected for simplicity. If the boundary forces are restricted to a fraction λ of a fixed traction pattern $\hat{\mathbf{t}}$, Eq. (1) defines a transformation from $(\hat{\mathbf{u}}, \hat{\mathbf{t}}, \mathbf{w})$ to the equilibrium path, which is then represented by $(\mathbf{u}, \lambda)$. This transformation will be referred to as the *mechanical transformation* and is represented by $\mathscr{T}$ in the sequel.

If the fields $(\hat{\mathbf{u}}, \hat{\mathbf{t}}, \mathbf{w})$ include random quantities, the equilibrium path and any characteristic Q of it is random as well. The distribution of Q should be evaluated through the mechanical transformation $\mathscr{T}$. Since this transformation is of a functional nature, numerical approximations must be used in general. The original random fields $(\hat{\mathbf{U}}, \hat{\mathbf{T}}, \mathbf{W})$ are discretised into a vector of jointly distributed variables $\mathbf{V}$ (Li and Der Kiureghian, 1993). This is schematised in Fig. 1 for a generic field of material properties. The correlation coefficient of the variables $\mathbf{V}$ is obtained from the autocorrelation function of the random field $\mathbf{W}$. By means of adequate transformations (Nataf, 1962; Rosenblatt, 1952; Der Kiureghian and Liu, 1986; Ditlevsen and

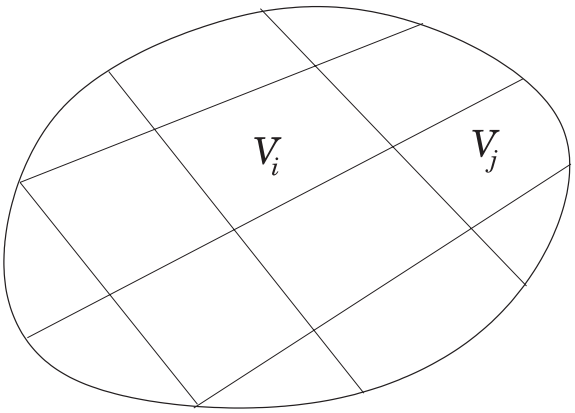

Fig. 1. Discretisation of the random field of material properties.

Madsen, 1996), the variables $\mathbf{V}$ can be converted into a set of uncorrelated, standard normally distributed variables $\mathbf{S}$. The cumulative distribution of Q can then be expressed as

$$\begin{aligned}\Pr(Q < q_0) &= \int_{q<q_0} f_Q(q)\,\mathrm{d}q \\ &= \int_{q(\mathbf{s})<q_0} \phi_n(\mathbf{s},\mathbf{I})\,\mathrm{d}\mathbf{s},\end{aligned} \tag{2}$$

where ϕ is the n-variate standard normal probability distribution function, $\mathbf{I}$ is the identity matrix and accounts for the correlation matrix of $\mathbf{S}$ in this context, and the dependence of q on $\mathbf{s}$ is provided by a (generally non-linear) finite element algorithm.

As the shape of the domain $q(\mathbf{s}) < q_0$ is non-linear, the integral proposed in Eq. (2) cannot be evaluated exactly. A traditional alternative is the Monte-Carlo method, the computational cost of which grows exorbitantly when the tails of the distribution of Q are studied. The essence of the finite element reliability method (Der Kiureghian and Ke, 1988) is to approximate the surface $q(\mathbf{s}) = q_0$ by low-order surfaces at the realisations of $\mathbf{S}$, which exhibit the largest probability density. The domain $q(\mathbf{s}) < q_0$ is consequently approximated by a number of subsets. The approximation points are referred to as β-points and are denoted by $\mathbf{s}^\beta$. The distance of these points to the origin is traditionally known as β-reliability index. If a linear approximation is used, the probability contribution of each approximating subset $\overline{q}_i(\mathbf{s}) < 0$ to the cumulative distribution of Q is given by

$$P_i = \Phi(-\beta_i), \tag{3}$$

where Φ represents the one-dimensional standard normal cumulative distribution function. The contribution of k subsets to the cumulative distribution of Q is given by the expression

$$P_{i_1,\ldots,i_k} = 1 - \Phi_k(\boldsymbol{\beta}, \boldsymbol{\rho}^\beta), \tag{4}$$

where Φ_k is the k-variate standard normal cumulative distribution function and $\boldsymbol{\beta}$ is a vector containing the k $\boldsymbol{\beta}$-indices considered. If the unitary $\boldsymbol{\alpha}$-vectors are introduced through the notation

$$\mathbf{s}^\beta = -\beta\boldsymbol{\alpha} \tag{5}$$

then the correlation matrix $\boldsymbol{\rho}^\beta$ of the approximating subsets is obtained from

$$\rho^{\beta}_{i_l i_m} = \boldsymbol{\alpha}^{\mathrm{T}}_{i_l} \boldsymbol{\alpha}_{i_m}. \tag{6}$$

Direct evaluation of Eq. (4) can be costly when the dimension of $\boldsymbol{\beta}$ is large. As an alternative, bounds for $P_{i_1,\ldots,i_k}$ have been devised (Ditlevsen and Madsen, 1996) as well as first-order approximations (Hohenbichler and Rackwitz, 1983).

Finding the β-points is the main task in the reliability method. Due to the spherical symmetry of the uncorrelated standard normal space, the local maxima of the probability density function on $q(\mathbf{s}) = q_0$ coincide with the local minima of the distance of this surface to the origin. The computation of the β-points is consequently formulated as a constrained optimisation problem

$$\begin{cases} \text{minimise} & \|\mathbf{s}\|, \\ \text{subject to} & q(\mathbf{s}) = q_0. \end{cases} \tag{7}$$

The solution of this problem is found through an iterative algorithm in the form

$$\mathbf{s}^{(k+1)} = \mathscr{G}\left(\mathbf{s}^{(k)}, q^{(k)}, \frac{\partial q^{(k)}}{\partial \mathbf{s}}\right), \tag{8}$$

where k now accounts for the iteration number and $\mathscr{G}$ represents a suitable procedure. A comprehensive review of optimisation algorithms with the application to reliability problems can be found in Liu and Kiureghian (1991).

3. The mechanical transformation

3.1. Computation of the equilibrium path

A finite element discretisation of the governing equations can be obtained from the principle of virtual work,

$$\int_{\Omega} \delta\boldsymbol{\varepsilon}^{\mathrm{T}} \boldsymbol{\sigma}\, \mathrm{d}\Omega - \int_{\partial\Omega} \delta\mathbf{u}^{\mathrm{T}} \lambda \hat{\mathbf{t}}\, \mathrm{d}\Gamma = 0. \tag{9}$$

When the variation $\delta\mathbf{u}$ is not explicitly required to satisfy the constraints of $\hat{\mathbf{u}}$, these are imposed through Lagrange multipliers. In this study, it is considered that these constraints are present at the boundary and are given by a set of n affine relations

$$\mathbf{G}_i\mathbf{u} - \mathbf{g}_i = 0 \quad \text{on } \partial\Omega_i,\ i = 1, \ldots, n. \tag{10}$$

It is remarked that the subsets $\partial\Omega_i$ need not be connected and may overlap, as long as the constraints are mutually consistent. Incorporation of the essential boundary condition (10) into Eq. (9) leads to

$$\int_{\Omega} \delta\boldsymbol{\varepsilon}^{\mathrm{T}} \boldsymbol{\sigma}\, \mathrm{d}\Omega - \int_{\partial\Omega} \delta\mathbf{u}^{\mathrm{T}} \lambda \hat{\mathbf{t}}\, \mathrm{d}\Gamma + \sum_{i=1}^{n} \int_{\partial\Omega_i} \delta\left[\boldsymbol{\mu}_i^{\mathrm{T}} (\mathbf{G}_i\mathbf{u} - \mathbf{g}_i)\right] \mathrm{d}\Gamma = 0, \tag{11}$$

where $\boldsymbol{\mu}_i$ represents a set of Lagrange multipliers. Eq. (11) is reworked as

$$\int_{\Omega} \delta\boldsymbol{\varepsilon}^{\mathrm{T}} \boldsymbol{\sigma}\, \mathrm{d}\Omega - \int_{\partial\Omega} \delta\mathbf{u}^{\mathrm{T}} \lambda \hat{\mathbf{t}}\, \mathrm{d}\Gamma + \sum_{i=1}^{n} \left[\int_{\partial\Omega_i} \delta\boldsymbol{\mu}_i^{\mathrm{T}} (\mathbf{G}_i\mathbf{u} - \mathbf{g}_i)\, \mathrm{d}\Gamma + \int_{\partial\Omega_i} \delta\mathbf{u}^{\mathrm{T}} \mathbf{G}_i^{\mathrm{T}} \boldsymbol{\mu}_i\, \mathrm{d}\Gamma \right] = 0. \tag{12}$$

A discrete form of this condition is stated by expanding the displacement field in finite elements as

$$\mathbf{u} = \mathbf{N}\mathbf{a}. \tag{13}$$

The transformation from the displacement vector to the deformation tensor is represented as

$$\boldsymbol{\varepsilon} = \mathbf{L}\mathbf{u} \tag{14}$$

with $\mathbf{L}$ as the kinematic differential operator. Upon introduction of discretisation, Eq. (14) is expressed as

$$\begin{aligned}\boldsymbol{\varepsilon} &= \mathbf{L}\mathbf{N}\mathbf{a} \\ &= \mathbf{B}\mathbf{a},\end{aligned} \tag{15}$$

where the matrix $\mathbf{B}$ has been introduced that relates the deformation to discretisation coefficients. The Lagrange multipliers $\boldsymbol{\mu}_i$ are expanded in the same fashion

$$\boldsymbol{\mu} = \tilde{\mathbf{N}}\mathbf{m}. \tag{16}$$

Replacing terms in Eq. (12) leads to the expression

$$\int_{\Omega} \delta\mathbf{a}^{\mathrm{T}}\mathbf{B}^{\mathrm{T}}\boldsymbol{\sigma}\,\mathrm{d}\Omega - \int_{\partial\Omega} \delta\mathbf{a}^{\mathrm{T}}\lambda\mathbf{N}^{\mathrm{T}}\hat{\mathbf{t}}\,\mathrm{d}\Gamma + \int_{\partial\Omega} \delta\mathbf{m}^{\mathrm{T}}\tilde{\mathbf{N}}^{\mathrm{T}}(\mathbf{G}\mathbf{N}\mathbf{a} - \mathbf{g})\,\mathrm{d}\Gamma + \int_{\partial\Omega} \delta\mathbf{a}^{\mathrm{T}}\mathbf{N}^{\mathrm{T}}\mathbf{G}^{\mathrm{T}}\tilde{\mathbf{N}}\mathbf{m}\,\mathrm{d}\Gamma = 0. \tag{17}$$

Adopting the notations

$$\begin{aligned}\mathbf{f}^{\mathrm{int}} &= \int_{\Omega} \mathbf{B}^{\mathrm{T}}\boldsymbol{\sigma}\,\mathrm{d}\Omega, \\ \hat{\mathbf{f}} &= \int_{\partial\Omega} \mathbf{N}^{\mathrm{T}}\hat{\mathbf{t}}\,\mathrm{d}\Gamma, \\ \mathbf{A} &= \int_{\partial\Omega} \tilde{\mathbf{N}}^{\mathrm{T}}\mathbf{G}\mathbf{N}\,\mathrm{d}\Gamma, \\ \mathbf{b} &= \int_{\partial\Omega} \tilde{\mathbf{N}}^{\mathrm{T}}\mathbf{g}\,\mathrm{d}\Gamma,\end{aligned} \tag{18}$$

Eq. (17) is more conveniently expressed as

$$\delta\mathbf{a}^{\mathrm{T}}(\mathbf{f}^{\mathrm{int}} - \lambda\hat{\mathbf{f}} + \mathbf{A}^{\mathrm{T}}\mathbf{m}) + \delta\mathbf{m}^{\mathrm{T}}(\mathbf{A}\mathbf{a} - \mathbf{b}) = 0. \tag{19}$$

As relation (19) must hold for any variation $\delta\mathbf{a}$ and $\delta\mathbf{m}$, the equilibrium algebraic equations

$$\begin{aligned}\mathbf{f}^{\mathrm{int}} + \mathbf{A}^{\mathrm{T}}\mathbf{m} &= \lambda\hat{\mathbf{f}}, \\ \mathbf{A}\mathbf{a} &= \mathbf{b}\end{aligned} \tag{20}$$

result, which represent an implicit relation for the equilibrium path. Solution of Eq. (20) is usually obtained through an incremental procedure. The evolution of a generic quantity is represented by

$$^{\tau+\Delta\tau}\alpha = {}^{\tau}\alpha + \Delta\alpha, \tag{21}$$

where τ represents a path parameter, and a relation is introduced between the discretised incremental loading parameter $\Delta\lambda$ and the incremental displacements $\Delta\mathbf{a}$,

$$l(\Delta\mathbf{a}, \Delta\lambda; \Delta\tau) = 0. \tag{22}$$

Introducing a vector of residuals

$$\mathbf{r} = \begin{pmatrix} \Delta\mathbf{f}^{\mathrm{int}} + \mathbf{A}^{\mathrm{T}}\Delta\mathbf{m} - \Delta\lambda\hat{\mathbf{f}} \\ \mathbf{A}\Delta\mathbf{a} - \Delta\mathbf{b} \\ l(\Delta\mathbf{a}, \Delta\lambda; \Delta\tau) \end{pmatrix}, \tag{23}$$

the equilibrium path is computed with the Newton–Raphson method

$$\begin{pmatrix} \Delta\mathbf{a} \\ \Delta\mathbf{m} \\ \Delta\lambda \end{pmatrix}^{(k+1)} = \begin{pmatrix} \Delta\mathbf{a} \\ \Delta\mathbf{m} \\ \Delta\lambda \end{pmatrix}^{(k)} - \begin{bmatrix} \frac{\partial \Delta\mathbf{f}^{\text{int}}}{\partial \Delta\mathbf{a}} & \mathbf{A}^{\mathrm{T}} & -\hat{\mathbf{f}} \\ \mathbf{A} & \mathbf{0} & \mathbf{0} \\ \frac{\partial l}{\partial \Delta\mathbf{a}} & \mathbf{0} & \frac{\partial l}{\partial \Delta\lambda} \end{bmatrix}^{-1} \mathbf{r}^{(k)}, \tag{24}$$

where k stands for the iteration number. Procedure (24) is continued until convergence is attained with respect to a proper norm.

The relation between the vector of nodal internal forces and the nodal displacements is given, from a computational point of view, by an implicit relation

$$\mathbf{c}(\Delta\boldsymbol{\sigma}, \Delta\boldsymbol{\kappa}, {}^{\tau}\boldsymbol{\sigma}, {}^{\tau}\boldsymbol{\kappa}, \Delta\boldsymbol{\varepsilon}; \mathbf{w}) = \mathbf{0}, \tag{25}$$

where $\boldsymbol{\kappa}$ is a set of parameters representing the strain history. Eq. (25) requires the use of iterative algorithms in general to solve the increment of stress and history parameters, which correspond to an increment of strain. Implicit derivation of (25) provides the consistent tangent operator $\partial\Delta\boldsymbol{\sigma}/\partial\Delta\boldsymbol{\varepsilon}$, which is used in the Jacobian matrix of Eq. (24) as

$$\frac{\partial \Delta\mathbf{f}^{\text{int}}}{\partial \Delta\mathbf{a}} = \int_{\Omega} \mathbf{B}^{\mathrm{T}} \frac{\partial \Delta\boldsymbol{\sigma}}{\partial \Delta\boldsymbol{\varepsilon}} \mathbf{B}\, \mathrm{d}\Omega. \tag{26}$$

3.2. Differentiation of the equilibrium path

Execution of algorithm (8) requires the evaluation of the sensitivity of the measure q with respect to the realisations of the standard normal variables $\mathbf{s}$. This is formalised by means of the chain rule as

$$\frac{\partial q}{\partial \mathbf{s}} = \frac{\partial q}{\partial(\mathbf{u}, \lambda)} \frac{\partial(\mathbf{u}, \lambda)}{\partial \mathbf{v}} \frac{\partial \mathbf{v}}{\partial \mathbf{s}}. \tag{27}$$

The term $\partial q/\partial(\mathbf{u}, \lambda)$ can be obtained easily from the definition of q, and the term $\partial\mathbf{v}/\partial\mathbf{s}$ usually presents no problems. The major difficulties are found in the evaluation of the term $\partial(\mathbf{u}, \lambda)/\partial\mathbf{v}$. In general, the vector $\mathbf{V}$ represents the discretisation of the material properties $\mathbf{W}$, boundary constraints $\hat{\mathbf{U}}$ and traction pattern $\hat{\mathbf{T}}$. The evaluation of the sensitivity of the equilibrium path with respect to the material properties can be carried out efficiently on each converged state of the Eq. (20) (Kleiber and Kowalczyk, 1995). Theoretical and computational aspects of this evaluation for the particular case of softening solids can be found in Gutiérrez and De Borst (1998).

3.2.1. Differentiation with respect to the material properties

At a converged solution of the equilibrium path, residual (23) vanishes, that is

$$\begin{aligned} \Delta\mathbf{f}^{\text{int}} + \mathbf{A}^{\mathrm{T}}\Delta\mathbf{m} - \Delta\lambda\hat{\mathbf{f}} &= \mathbf{0}, \\ \mathbf{A}\Delta\mathbf{a} - \Delta\mathbf{b} &= \mathbf{0}, \\ l(\Delta\mathbf{a}, \Delta\lambda; \Delta\tau) &= 0. \end{aligned} \tag{28}$$

Differentiation of Eq. (28) with respect to $\mathbf{v}$ yields

$$\begin{aligned} \frac{\partial}{\partial \mathbf{v}} \Delta\mathbf{f}^{\text{int}} + \mathbf{A}^{\mathrm{T}} \frac{\partial}{\partial \mathbf{v}} \Delta\mathbf{m} - \hat{\mathbf{f}} \frac{\partial}{\partial \mathbf{v}} \Delta\lambda &= \mathbf{0}, \\ \mathbf{A} \frac{\partial}{\partial \mathbf{v}} \Delta\mathbf{a} &= \mathbf{0}, \\ \frac{\partial l}{\partial \Delta\mathbf{a}} \frac{\partial}{\partial \mathbf{v}} \Delta\mathbf{a} + \frac{\partial l}{\partial \Delta\lambda} \frac{\partial}{\partial \mathbf{v}} \Delta\lambda &= 0. \end{aligned} \tag{29}$$

The derivative of the increment of internal forces in Eq. (29) is developed as

$$\frac{\partial}{\partial \mathbf{v}} \Delta \mathbf{f}^{\text{int}} = \int_{\Omega} \mathbf{B}^{\mathrm{T}} \frac{\partial}{\partial \mathbf{v}} \Delta \boldsymbol{\sigma} \, \mathrm{d}\Omega. \tag{30}$$

The derivative of the stress increment with respect to $\mathbf{v}$ can be decomposed into two contributions

$$\frac{\partial}{\partial \mathbf{v}} \Delta \boldsymbol{\sigma} = \frac{\partial}{\partial \mathbf{v}} \Delta \boldsymbol{\sigma} \bigg|_{\Delta \varepsilon} + \frac{\partial \Delta \boldsymbol{\sigma}}{\partial \Delta \boldsymbol{\varepsilon}} \frac{\partial}{\partial \mathbf{v}} \Delta \boldsymbol{\varepsilon}, \tag{31}$$

where the term $\partial \Delta \boldsymbol{\sigma} / \partial \Delta \boldsymbol{\varepsilon}$ is recognised as the consistent tangent operator introduced in Eq. (26). Using the relation $(\partial/\partial \mathbf{v}) \Delta \boldsymbol{\varepsilon} = \mathbf{B} (\partial/\partial \mathbf{v}) \Delta \mathbf{a}$, Eqs. (29)–(31) form a system of linear simultaneous equations that can be recast as

$$\begin{bmatrix} \mathbf{K} & \mathbf{A}^{\mathrm{T}} & -\hat{\mathbf{f}} \\ \mathbf{A} & \mathbf{0} & \mathbf{0} \\ \frac{\partial l}{\partial \Delta \mathbf{a}} & \mathbf{0} & \frac{\partial l}{\partial \Delta \lambda} \end{bmatrix} \begin{pmatrix} \frac{\partial}{\partial \mathbf{v}} \Delta \mathbf{a} \\ \frac{\partial}{\partial \mathbf{v}} \Delta \mathbf{m} \\ \frac{\partial}{\partial \mathbf{v}} \Delta \lambda \end{pmatrix} = \begin{pmatrix} -\int_{\Omega} \mathbf{B}^{\mathrm{T}} \frac{\partial}{\partial \mathbf{v}} \Delta \boldsymbol{\sigma} \big|_{\Delta \varepsilon} \, \mathrm{d}\Omega \\ \mathbf{0} \\ 0 \end{pmatrix}. \tag{32}$$

The first term of the right-hand side of Eq. (32) is obtained by differentiating Eq. (25) with respect to $\mathbf{v}$ for constant $\Delta \boldsymbol{\varepsilon}$,

$$\begin{bmatrix} \frac{\partial \mathbf{c}}{\partial \Delta \boldsymbol{\sigma}} & \frac{\partial \mathbf{c}}{\partial \Delta \boldsymbol{\kappa}} \end{bmatrix} \begin{pmatrix} \frac{\partial}{\partial \mathbf{v}} \Delta \boldsymbol{\sigma} \big|_{\Delta \varepsilon} \\ \frac{\partial}{\partial \mathbf{v}} \Delta \boldsymbol{\kappa} \big|_{\Delta \varepsilon} \end{pmatrix} = - \begin{bmatrix} \frac{\partial \mathbf{c}}{\partial {}^{\tau}\boldsymbol{\sigma}} & \frac{\partial \mathbf{c}}{\partial {}^{\tau}\boldsymbol{\kappa}} & \frac{\partial \mathbf{c}}{\partial \mathbf{w}} \end{bmatrix} \begin{pmatrix} \frac{\partial}{\partial \mathbf{v}} {}^{\tau}\boldsymbol{\sigma} \\ \frac{\partial}{\partial \mathbf{v}} {}^{\tau}\boldsymbol{\kappa} \\ \frac{\partial}{\partial \mathbf{v}} \mathbf{w} \end{pmatrix}, \tag{33}$$

and solving for $(\partial/\partial \mathbf{v}) \Delta \boldsymbol{\sigma}|_{\Delta \varepsilon}$. The terms $(\partial/\partial \mathbf{v})^{\tau} \boldsymbol{\sigma}$ and $(\partial/\partial \mathbf{v})^{\tau} \boldsymbol{\kappa}$ are known from the previous loading step and introduce the effects of the deformation history in the computation of the derivatives. The term $(\partial/\partial \mathbf{v}) \mathbf{w}$ depends on the spatial coordinate of the integration point considered.

Next, solution of Eq. (32) provides the derivatives $(\partial/\partial \mathbf{v}) \Delta \mathbf{a}$, $(\partial/\partial \mathbf{v}) \Delta \mathbf{m}$ and $(\partial/\partial \mathbf{v}) \Delta \lambda$. Through the relation $\boldsymbol{\varepsilon} = \mathbf{B}\mathbf{a}$, the derivatives are computed of the incremental deformation tensor $(\partial/\partial \mathbf{v}) \Delta \boldsymbol{\varepsilon}$ and, subsequently, those of $\Delta \boldsymbol{\sigma}$ and $\Delta \boldsymbol{\kappa}$ by differentiating the constitutive relation (25).

By means of updating relation (21), the derivatives $(\partial/\partial \mathbf{v})^{\tau+\Delta\tau} \mathbf{a}$, $(\partial/\partial \mathbf{v})^{\tau+\Delta\tau} \mathbf{m}$ and $(\partial/\partial \mathbf{v})^{\tau+\Delta\tau} \lambda$ are computed. Similarly, the derivatives of ${}^{\tau+\Delta\tau}\boldsymbol{\sigma}$ and ${}^{\tau+\Delta\tau}\boldsymbol{\kappa}$ are updated for use in Eq. (33) in the next loading step.

3.2.2. Differentiation with respect to the boundary constraints

Following the same strategy as for the material properties, derivatives can be computed of the equilibrium path with respect to the boundary constraints if these have been imposed through Lagrange multipliers. In the ensuing development, the boundary constraints are represented in the discrete form elaborated in Section 3.1

$$\mathbf{A}\mathbf{a} - \mathbf{b} = \mathbf{0}. \tag{34}$$

Only the computation of derivatives with respect to $\mathbf{b}$ is considered in this study. An extension of this development to handle derivatives of components of $\mathbf{A}$ is straightforward.

The formulation presented in the previous section is used again to evaluate the derivatives with respect to $\mathbf{b}$. The terms $\partial \mathbf{c}/\partial \mathbf{w}$ and $(\partial/\partial \mathbf{v}) \mathbf{w}$ disappear from Eq. (33), which attains the form

$$\begin{bmatrix} \frac{\partial \mathbf{c}}{\partial \Delta \boldsymbol{\sigma}} & \frac{\partial \mathbf{c}}{\partial \Delta \boldsymbol{\kappa}} \end{bmatrix} \begin{pmatrix} \frac{\partial}{\partial \mathbf{b}} \Delta \boldsymbol{\sigma} \big|_{\Delta \varepsilon} \\ \frac{\partial}{\partial \mathbf{b}} \Delta \boldsymbol{\kappa} \big|_{\Delta \varepsilon} \end{pmatrix} = - \begin{bmatrix} \frac{\partial \mathbf{c}}{\partial {}^{\tau}\boldsymbol{\sigma}} & \frac{\partial \mathbf{c}}{\partial {}^{\tau}\boldsymbol{\kappa}} \end{bmatrix} \begin{pmatrix} \frac{\partial}{\partial \mathbf{b}} {}^{\tau}\boldsymbol{\sigma} \\ \frac{\partial}{\partial \mathbf{b}} {}^{\tau}\boldsymbol{\kappa} \end{pmatrix}. \tag{35}$$

At the first loading step, the second expression in Eq. (29), which accounts for the differentiated version of Eq. (34), must include the derivatives of $\mathbf{b}$ and consequently attains the form

$$\mathbf{A}\frac{\partial}{\partial \mathbf{b}}\Delta\mathbf{a} = \mathbf{I}. \tag{36}$$

Similarly, since both $(\partial/\partial\mathbf{b})^0\boldsymbol{\sigma}$ and $(\partial/\partial\mathbf{b})^0\boldsymbol{\kappa}$ vanish, the term $(\partial/\partial\mathbf{b})\Delta\boldsymbol{\sigma}|_{\Delta\varepsilon}$ obtained from Eq. (35) vanishes as well. The counterpart of Eq. (32) thus reads

$$\begin{bmatrix} \mathbf{K} & \mathbf{A}^{\mathrm{T}} & -\hat{\mathbf{f}} \\ \mathbf{A} & \mathbf{0} & \mathbf{0} \\ \frac{\partial l}{\partial \Delta\mathbf{a}} & \mathbf{0} & \frac{\partial l}{\partial \Delta\lambda} \end{bmatrix} \begin{pmatrix} \frac{\partial}{\partial \mathbf{b}}\Delta\mathbf{a} \\ \frac{\partial}{\partial \mathbf{b}}\Delta\mathbf{m} \\ \frac{\partial}{\partial \mathbf{b}}\Delta\lambda \end{pmatrix} = \begin{pmatrix} \mathbf{0} \\ \mathbf{I} \\ 0 \end{pmatrix}, \tag{37}$$

and its solution yields the derivatives of the equilibrium path with respect to $\mathbf{b}$ at the first loading step. At the subsequent steps, the constraint equation is of the form

$$\mathbf{A}\Delta\mathbf{a} = \mathbf{0} \tag{38}$$

while the derivatives $(\partial/\partial\mathbf{b})^{\tau}\boldsymbol{\sigma}$ and $(\partial/\partial\mathbf{b})^{\tau}\boldsymbol{\kappa}$ are non-zero. Consequently, the term $(\partial/\partial\mathbf{b})\Delta\boldsymbol{\sigma}|_{\Delta\varepsilon}$ is also non-zero and the incremental derivatives of the equilibrium path are obtained from

$$\begin{bmatrix} \mathbf{K} & \mathbf{A}^{\mathrm{T}} & -\hat{\mathbf{f}} \\ \mathbf{A} & \mathbf{0} & \mathbf{0} \\ \frac{\partial l}{\partial \Delta\mathbf{a}} & \mathbf{0} & \frac{\partial l}{\partial \Delta\lambda} \end{bmatrix} \begin{pmatrix} \frac{\partial}{\partial \mathbf{b}}\Delta\mathbf{a} \\ \frac{\partial}{\partial \mathbf{b}}\Delta\mathbf{m} \\ \frac{\partial}{\partial \mathbf{b}}\Delta\lambda \end{pmatrix} = \begin{pmatrix} -\int_{\Omega} \mathbf{B}^{\mathrm{T}} \frac{\partial}{\partial \mathbf{b}}\Delta\boldsymbol{\sigma}\big|_{\Delta\varepsilon}\,\mathrm{d}\Omega \\ \mathbf{0} \\ 0 \end{pmatrix}. \tag{39}$$

The total derivatives of the equilibrium path as well as those of the internal variables are updated as in the previous section, by means of Eq. (21).

4. Strain localisation in viscoplastic solids

The relation between material heterogeneity and shear band patterning is studied by means of the biaxial tension test of Fig. 2. This kind of (tension or compression) biaxial tests have been the subject of several experimental (Desrues (1984) among others) as well as numerical studies (De Borst, 1989, 1993; Sluys, 1992, among others). A relevant characteristic of this problem from a computational point of view is that an imperfection is needed in order to trigger localisation. Such an imperfection is usually supplied by reducing the strength within a patch of finite elements. The computed equilibrium path is obviously dependent on the chosen imperfection and the objectivity of the calculation is therefore questionable. Since the actual localisation pattern observed in experiments is determined by the ductility and heterogeneity, it is meaningful to consider a random distribution of the material properties field, and by means of the techniques described in this paper, to study the statistics of the equilibrium path.

The specimen considered has a size of 120×60 mm^2, a thickness of 5 mm and is composed of a von Mises, Duvaut–Lions viscoplastic material (Duvaut and Lions, 1972). The constitutive equations of this model are expressed as

$$\begin{aligned} \dot{\boldsymbol{\sigma}} &= \mathbf{D}\dot{\boldsymbol{\varepsilon}} - \frac{1}{\zeta}(\boldsymbol{\sigma} - \boldsymbol{\sigma}^p), \\ \dot{\kappa} &= -\frac{1}{\zeta}(\kappa - \kappa^p), \end{aligned} \tag{40}$$

where ζ is a relaxation time related to the viscosity, and $\boldsymbol{\sigma}^p$ and $\boldsymbol{\kappa}^p$ are the stress tensor and history parameters corresponding to a standard, rate-independent plasticity model. These equations are valid when the yield function is positive

$$f(\boldsymbol{\sigma}, \kappa) > 0 \tag{41}$$

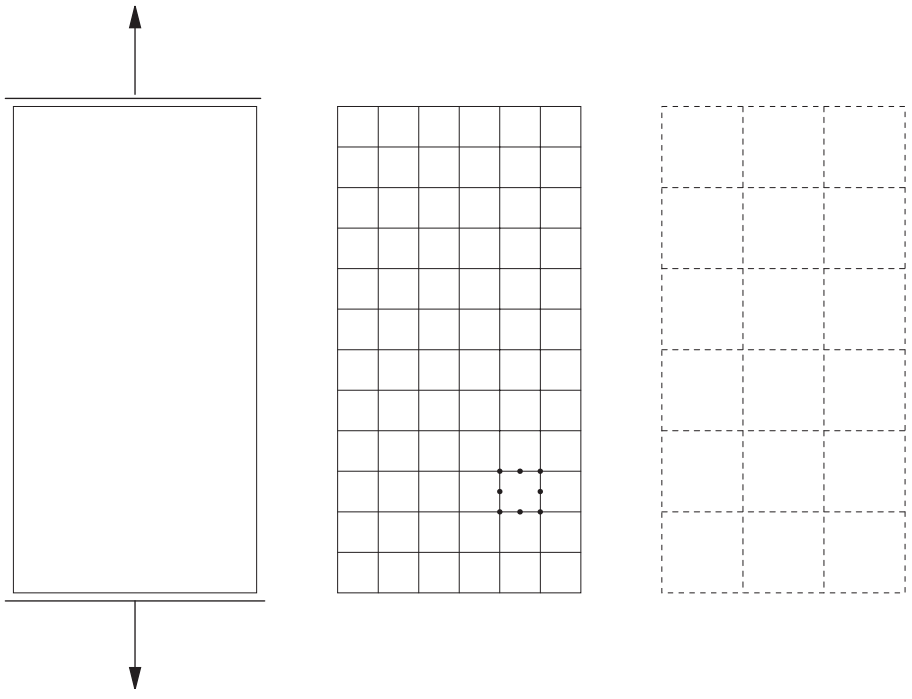

Fig. 2. Biaxial tension test: static scheme, finite element mesh and random field mesh.

otherwise, the material point is in the elastic regime

$$\dot{\boldsymbol{\sigma}} = \mathbf{D}\dot{\boldsymbol{\varepsilon}}. \tag{42}$$

The computation of the equilibrium path and the sensitivity to the material properties has been elaborated in Gutiérrez and De Borst (1998, 1999a). The domain is discretised into a structured mesh of 28×14 eight-noded, plane-stress finite elements with a four-point Gauss–Legendre integration quadrature. Linear constraint equations are used at the top and bottom to ensure that both boundaries remain parallel during the loading process, which is controlled by an indirect displacement control procedure such that the distance between both ends increases with a velocity of 1 mm/s.

Young's modulus and the initial yield stress are logarithmic-normally distributed according to the medians

$$\begin{aligned} Y_m &= 20\,000 \text{ N/mm}^2, \\ \overline{\Sigma}_{0m} &= 100 \text{ N/mm}^2. \end{aligned} \tag{43}$$

The hardening (softening) modulus obeys a normal distribution with

$$\mu_H = -500 \text{ N/mm}^2. \tag{44}$$

The coefficient of variation is $\mathscr{C} = 0.1$ for all properties and an exponential autocorrelation function with the correlation length $l_c = 20$ mm is considered. Each random field is discretised into 98 subdomains corresponding with patches of 2×2 finite elements. Poisson's ratio has been taken to be $\nu = 0.2$.

The energy dissipation in the time interval $[0 \text{ s}, 0.75 \text{ s}]$ is studied. A generic energy dissipation threshold $\psi_0 = 12\,000$ N mm is considered and the adopted time step is $\Delta t = 0.0125$ s. Symmetric or asymmetric

β-points are found by starting optimisation algorithm (8) from symmetric or asymmetric realisations, respectively.

For the relaxation time $\zeta = 0.0015$ s, the asymmetric β-points have $\beta_a = 3.6693$, which corresponds to a joint probability $P_a = 2.29 \times 10^{-4}$. The correlation coefficient of the approximating failure subsets is $\rho = 0.68$. The symmetric β-point exhibits $\beta_s = 4.085$, which indicates a probability $P_s = 2.20 \times 10^{-5}$ for the symmetric mode. It is observed that the probabilistic contribution of the asymmetric modes is 10 times larger than that of the symmetric mode. The respective profiles of shear bands are presented in Fig. 3.

If the relaxation time is increased to $\zeta = 0.0030$ s, the correlation coefficient of the two homologous, asymmetric shear bands becomes $\rho = 0.84$. With the computed $\beta_a = 4.2715$, this leads to a probability contribution $P_a = 1.76 \times 10^{-5}$. The asymmetric mode is found at a distance $\beta_s = 4.3489$, which is in the same order of magnitude as β_a and provides a contribution $P_s = 6.84 \times 10^{-6}$. The width of the shear bands (Fig. 4) is increased with respect to the case $\zeta = 0.0015$ s.

If a larger relaxation time ($\zeta = 0.0045$ s) is considered, the computed β-points are closer to each other. The reliability indices now read $\beta_a = 4.4598$ and $\beta_s = 4.4578$, and the correlation coefficient of the homologous asymmetric points is $\rho = 0.93$. The probability contribution of the asymmetric modes is reduced to $P_a = 6.56 \times 10^{-6}$ and that of the symmetric mode remains in the same order of magnitude as in the previous case, $P_s = 4.14 \times 10^{-6}$. The resulting localisation patterns are shown in Fig. 5.

It is observed that larger relaxation times lead to lower probabilistic contributions to the energy dissipation. This result could be expected, since a larger relaxation time usually corresponds to a larger energy dissipation during failure.

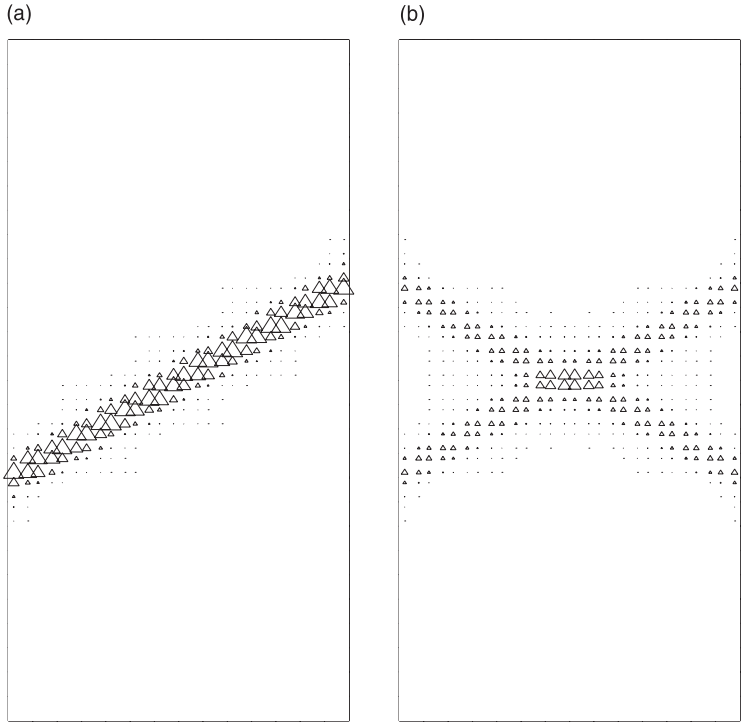

Fig. 3. Analysis of energy dissipation: profiles of equivalent plastic strain at the asymmetric (left) and the symmetric (right) β-points with $\zeta = 0.0015$ s.

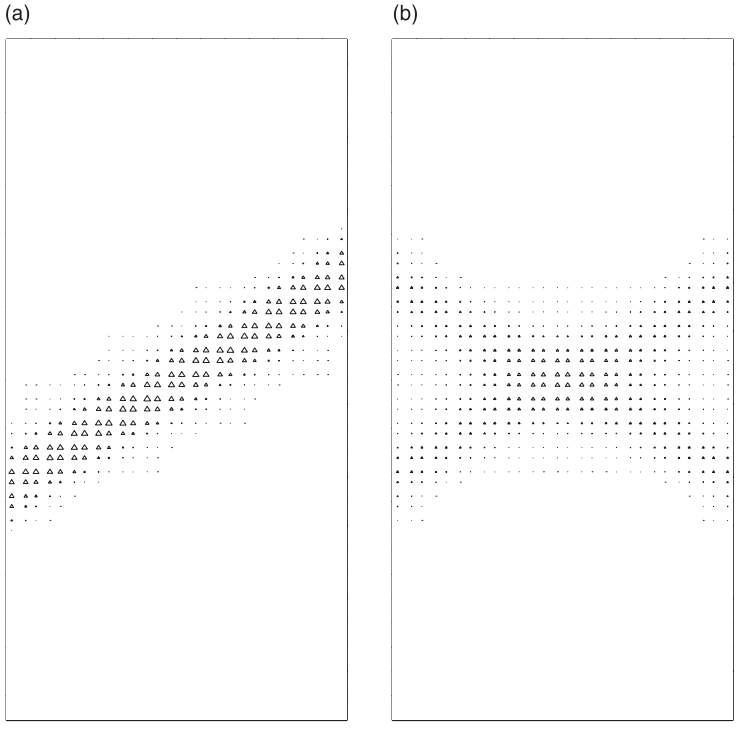

Fig. 4. Analysis of energy dissipation: profiles of equivalent plastic strain at the asymmetric (left) and the symmetric (right) β-points with $\zeta = 0.0030$ s.

5. Damage localisation in quasi-brittle materials

The influence of randomness of the boundary constraints in the evolution of damage is studied for a tensile test on a double-edge-notched specimen of concrete. The static scheme is depicted in Fig. 6. Experience has shown (Hordijk, 1991; Schlangen, 1993; van Mier, 1997) that such tests are sensitive to the boundary conditions. If the loading platens are kept fixed and if no extra imperfection is imposed, finite element simulations of this test exhibit a symmetric evolution of damage from both notches. Numerical inaccuracies, however, tend to break this symmetry during the post-peak branch. This observation is consistent with the unstable behaviour argumented by Bažant and Cedolin (1991) and by Rots and De Borst (1989). On the other hand, experiments show that the deformation pattern is usually asymmetric after the peak load is reached, and evolves to a symmetric pattern upon further deformation. If the loading platens are allowed to rotate, usually asymmetric evolutions of damage from one notch are observed. This behaviour has successfully been reproduced by means of the finite element reliability method (Gutiérrez and De Borst, 1999b). The results presented in that are complemented in this paper by including the influence of errors in the horizontality of fixed loading platens.

A gradient-enhanced damage model (Peerlíngs et al., 1996) is adopted. The stress–deformation relation is expressed as

$$\boldsymbol{\sigma} = (1 - \omega)\mathbf{D}\boldsymbol{\varepsilon}, \tag{45}$$

where $\omega \in [0, 1]$ is a damage parameter that is a function of a history parameter κ. This history parameter is formalised by the Kuhn–Tucker conditions,

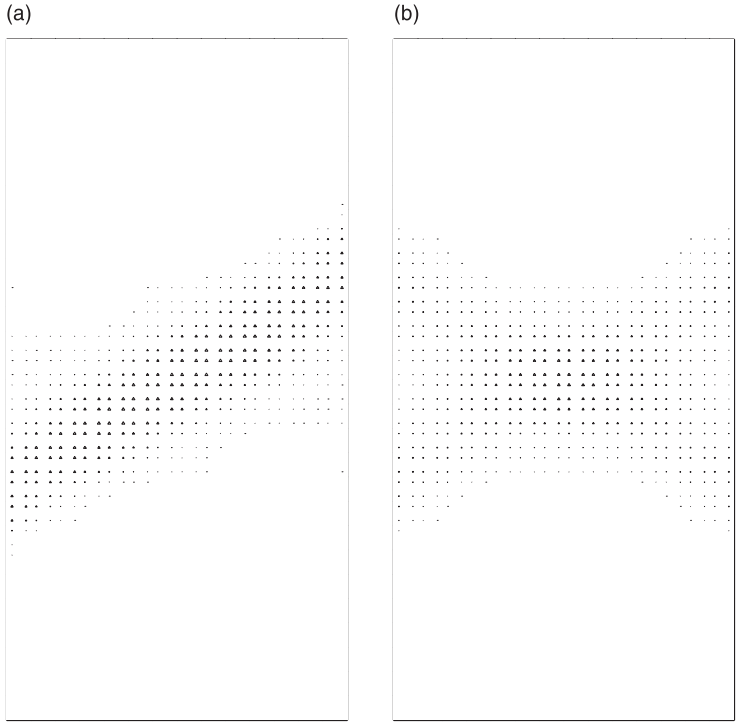

Fig. 5. Analysis of energy dissipation: profiles of equivalent plastic strain at the asymmetric (left) and the symmetric (right) β-points with $\zeta = 0.0045$ s.

$$\dot{\kappa} \geqslant 0 \qquad \overline{\varepsilon}^{\mathrm{eq}} - \kappa \leqslant 0 \qquad \dot{\kappa}(\overline{\varepsilon}^{\mathrm{eq}} - \kappa) = 0, \tag{46}$$

in which $\overline{\varepsilon}^{\mathrm{eq}}$ represents an averaged measure of the equivalent strain $\varepsilon^{\mathrm{eq}}$ and is obtained from the diffusion equation

$$\overline{\varepsilon}^{\mathrm{eq}} - \frac{1}{2} l_{\mathrm{s}}^2 \nabla^2 \overline{\varepsilon}^{\mathrm{eq}} = \varepsilon^{\mathrm{eq}}. \tag{47}$$

The parameter l_{s} is an internal length scale which quantifies the size of the zone in which damage evolves.

Following Gutiérrez and De Borst (1999b), Young's modulus has been taken to be $E = 18\,000$ MPa, $v = 0.2$, and the coefficients a and b governing the damage evolution law,

$$\omega(\kappa, \kappa_0) = \begin{cases} 1 - \frac{\kappa_0}{\kappa}[(1-a) + a\exp(-b(\kappa - \kappa_0))] & \text{if } \kappa > \kappa_0, \\ 0 & \text{otherwise,} \end{cases} \tag{48}$$

are $a = 0.96$ and $b = 350$. The parameter ξ controls the sensitivity to tension with respect to that in compression in the definition of the equivalent strain

$$\varepsilon^{\mathrm{eq}} = \frac{\xi - 1}{2\xi(1-2v)} I_1 + \frac{1}{2\xi}\sqrt{\frac{(\xi-1)^2}{(1-2v)^2} I_1^2 + \frac{2\xi}{(1+v)^2} J_2}, \tag{49}$$

where the strain tensor invariants are given by

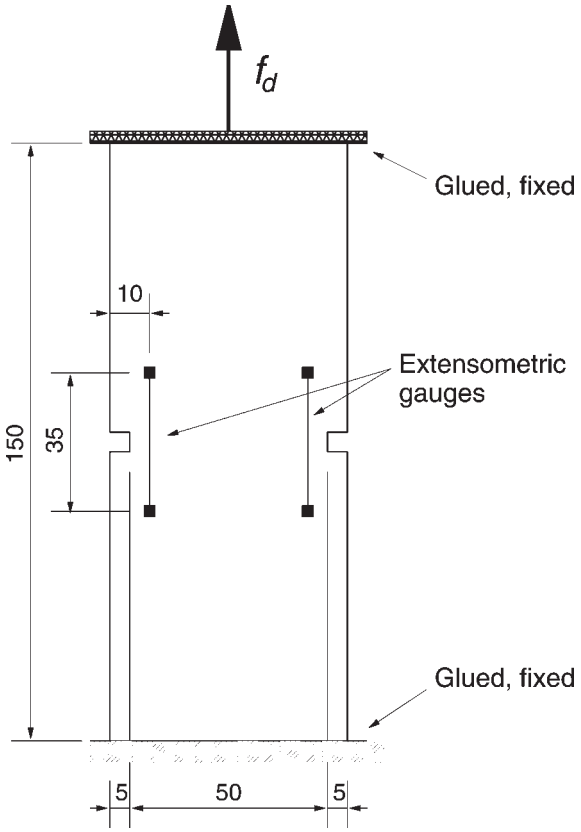

Fig. 6. Schematic representation of a tensile test on a double-edge-notched specimen (dimensions in mm).

$$I_1 = \varepsilon_1 + \varepsilon_2 + \varepsilon_3, \qquad (50)$$
$$J_2 = (\varepsilon_1 - \varepsilon_2)^2 + (\varepsilon_2 - \varepsilon_3)^2 + (\varepsilon_3 - \varepsilon_1)^2,$$

and it is taken as $\xi = 10$. The threshold for damage initiation is considered to follow a Weibull distribution according to the parameters

$$\kappa_0^{\min} = 1.5 \times 10^{-4}, \quad u = 2.1 \times 10^{-4}, \quad k = 2, \qquad (51)$$

and an exponential correlation function is used with a correlation length $l_c = 10$ mm.

The relative deformation of the extensometric gauges depicted in Fig. 6 can be used to define a state function as

$$Z(\Delta_l, \Delta_r) = \frac{\Delta_r - \Delta_l}{(\Delta_r + \Delta_l)/2}, \qquad (52)$$

where Δ_r and Δ_l represent the random extensions of the right and the left gauge, respectively. The denominator in (52) equals the path parameter τ, as a consequence of the simulated loading servo control. Different points of the cumulative distribution function of Z can be obtained by running algorithm (8) for

different threshold values z_0. Due to the symmetry of the problem, it is meaningful to study the probability that the absolute value of difference (52) exceeds the threshold. A first-order approximation of this probability is readily expressed as

$$\begin{aligned}\Pr(|Z| > z_0) &= \Pr(Z < -z_0) + \Pr(Z > z_0) \\ &\approx 2\Phi(-\beta).\end{aligned} \tag{53}$$

The statistics of the relative difference of gauge extensions has been studied at two different stages of the post-peak equilibrium path, namely for $(\delta_r + \delta_l)/2 = 0.008$ mm and $(\delta_r + \delta_l)/2 = 0.014$ mm, which approximately correspond to 100% and 75% of the peak load, respectively. In the first simulation, it has been assumed that the upper platen is perfectly horizontal. The results, which are shown in Table 1, show that the probability of exceeding a certain degree of asymmetry (quantified by z_0) decreases as the average deformation progresses.

In practice, the upper platen is not perfectly horizontal. The influence of a possible horizontality error can be computed by considering that the inhomogeneous term of the selected constraint equations is randomly distributed. In this case, it is considered that the difference q between the vertical displacement of the upper corners is normally distributed with mean $\mu_Q = 0$ mm. Two standard deviations $\sigma_Q = 5 \times 10^{-4}$ mm and $\sigma_Q = 5 \times 10^{-3}$ mm have been studied. For the small value of σ_Q, the statistics of the damage evolution, which are summarised in Table 2, do not essentially differ from those obtained with a perfectly horizontal plate.

A dramatic increase of the asymmetry probability is, however, observed when the scatter of the horizontality error is increased to $\sigma_Q = 5 \times 10^{-3}$ mm (Table 3). For the particular case $(\delta_r + \delta_l)/2 = 0.014$ mm

Table 1
Analysis of damage evolution: results for perfectly horizontal loading platen

$(\delta_r + \delta_l)/2$ (mm)	z_0	β	$\Pr(\|Z\| > z_0)$
0.008	0.3	0.817	0.414
	0.15	0.397	0.692
0.014	0.3	1.135	0.256
	0.15	0.572	0.568

Table 2
Analysis of damage evolution: results for horizontality error in the loading platen with $\sigma_Q = 5 \times 10^{-4}$ mm

$(\delta_r + \delta_l)/2$ (mm)	z_0	β	$\Pr(\|Z\| > z_0)$
0.008	0.3	0.805	0.420
	0.15	0.392	0.694
0.014	0.3	1.119	0.264
	0.15	0.562	0.574

Table 3
Analysis of damage evolution: results for horizontality error in the loading platen with $\sigma_Q = 5 \times 10^{-3}$ mm

$(\delta_r + \delta_l)/2$ (mm)	z_0	β	$\Pr(\|Z\| > z_0)$
0.008	0.3	0.421	0.674
	0.15	0.207	0.836
0.014	0.3	0.570	0.562
	0.15	0.285	0.776

and $z_0 = 0.30$, the cumulative distribution of the asymmetry is doubled. This result shows that small defects in the orientation of the loading plate can be of capital importance for the asymmetry in the evolution of the damage pattern during failure.

6. Conclusions

Stochastic aspects of localised strain or damage can be evaluated with the finite element reliability method. The influence of material as well as boundary constraint imperfections can be studied. In particular, stochastic boundary constraints can be considered in an efficient manner if they are imposed through Lagrange multipliers. The evaluation of the sensitivity to the basic random variables, which is needed in the reliability method, is straightforward. Numerical simulations of mode-I as well as mode-II localisation phenomena demonstrate how the introduction of stochastic concepts reveals phenomena that otherwise would remain unnoticed.

References

Barlow, J., 1982. Constraint relationships in linear and nonlinear finite element analyses. Int. J. Numer. Meth. Engng. 18, 521–533.
Bažant, Z.P., Cedolin, L., 1991. Stability of Structures. Oxford University Press, New York.
De Borst, R., 1989. Numerical methods for bifurcation analysis in geomechanics. Ingenieur-Archiv 59, 160–174.
De Borst, R., Sluys, L.J., Mühlhaus, H.-B., Pamin, J., 1993. Fundamental issues in finite element analyses of localization of deformation. Engng. Comp. 10, 99–121.
Der Kiureghian, A., Liu, P.L., 1986. Structural reliability under incomplete probability information. ASCE J. Engng. Mech. 112, 85–104.
Der Kiureghian, A., Ke, J.B., 1988. The stochastic finite element method in structural reliability. Prob. Engng. Mech. 3, 83–91.
Desrues, J., 1984. La localisation de la déformation dans les matériaux granulaires. Dissertation, ISM-INP Grenoble.
Ditlevsen, O., Madsen, H.O., 1996. Structural Reliability Methods. Wiley, Chichester.
Duvaut, G., Lions, J.L., 1972. Les inéquations en mécanique et en physique. Dunod, Paris.
Gutiérrez, M.A., 1999. Objective simulation of failure in heterogeneous softening solids. Dissertation, Delft University of Technology.
Gutiérrez, M.A., De Borst, R., 1998. Studies in material parameter sensitivity of softening solids. Comp. Meth. Appl. Mech. Engng. 162, 337–350.
Gutiérrez, M.A., De Borst, R., 1999a. Numerical analysis of localization using a viscoplastic regularization: influence of stochastic material defects. Int. J. Numer. Meth. Engng. 44, 1823–1841.
Gutiérrez, M.A., De Borst, R., 1999b. Deterministic and stochastic analysis of size effects and damage evolution in quasi-brittle materials. Arch. Appl. Mech. 69, 655–676.
Hohenbichler, M., Rackwitz, R., 1983. First-order concepts in system reliability. Struct. Safety 1, 177–188.
Hordijk, D.A., 1991. Local approach to fatigue of concrete. Dissertation, Delft University of Technology.
Kleiber, M., Kowalczyk, P., 1995. Constitutive parameter sensitivity in elasto-plasticity. Comp. Mech., 17, 36–48.
Li, C.C., Der Kiureghian, A., 1993. Optimal discretization of random fields. ASCE J. Engng. Mech. 119, 1136–1154.
Liu, P.L., Der Kiureghian, A., 1991. Optimization algorithms for structural reliability. Struct. Safety 9, 161–177.
Mier, J. van 1997. Fracture Processes of Concrete. CRC Press, Boca Raton.
Nataf, A., 1962. Détermination des distribution dont les marges sont données. Comptes rendus de l'Academie de Sciences 225, 42–43.
Peerlings, R., De Borst, R., Brekelmans, W.A.M., De Vree, J.H.P., 1996. Gradient enhanced damage for quasi-brittle materials. Int. J. Numer. Meth. Engng. 39, 3391–3403.
Rodríguez-Ferran, A., Huerta, A., 1999. Adapting Broyden method to handle linear constraints imposed via Lagrange multipliers. Int. J. Numer. Meth. Engng. 46, 2011–2026.
Rosenblatt, M., 1952. Remarks on a multivariate transformation. Ann. Math. Stat. 23, 470–472.
Rots, J.G., De Borst, R., 1989. Analysis of concrete fracture processes in "direct" tension. Int. J. Solids Struct. 25 (12), 1381–1394.
Schlangen, E., 1993. Experimental and numerical analysis of fracture processes in concrete. Dissertation, Delft University of Technology.
Schreyer, H.L., Parsons, D.A., 1995. Direct application of constraints to symmetric algebraic systems. Comm. Numer. Meth. Engng. 11, 563–573.
Sluys, L.J., 1992. Wave propagation, localization and dispersion in softening solids. Dissertation, Delft University of Technology.